Myosins XI modulate host cellular responses and penetration resistance to fungal pathogens

Long Yang[a,b], Li Qin[a], Guosheng Liu[a], Valera V. Peremyslov[c], Valerian V. Dolja[c], and Yangdou Wei[a,1]

[a]Department of Biology, University of Saskatchewan, Saskatoon, SK, Canada S7N 5E2; [b]State Key Laboratory of Agricultural Microbiology, Key Laboratory of Plant Pathology of Hubei Province, Huazhong Agricultural University, Wuhan 430070, China; and [c]Department of Botany and Plant Pathology and Center for Genome Research and Biocomputing, Oregon State University, Corvallis, OR 97331

Edited by Paul Schulze-Lefert, Max Planck Institute for Plant Breeding Research, Cologne, Germany, and approved August 14, 2014 (received for review March 21, 2014)

The rapid reorganization and polarization of actin filaments (AFs) toward the pathogen penetration site is one of the earliest cellular responses, yet the regulatory mechanism of AF dynamics is poorly understood. Using live-cell imaging in *Arabidopsis*, we show that polarization coupled with AF bundling involves precise spatiotemporal control at the site of attempted penetration by the nonadapted barley powdery mildew fungus, *Blumeria graminis* f. sp. *hordei* (*Bgh*). We further show that the *Bgh*-triggered AF mobility and organelle aggregation are predominately driven by the myosin motor proteins. Inactivation of myosins by pharmacological inhibitors prevents bulk aggregation of organelles and blocks recruitment of lignin-like compounds to the penetration site and deposition of callose and defensive protein, PENETRATION 1 (PEN1) into the apoplastic papillae, resulting in attenuation of penetration resistance. Using gene knockout analysis, we demonstrate that highly expressed myosins XI, especially myosin XI-K, are the primary contributors to cell wall-mediated penetration resistance. Moreover, the quadruple myosin knockout mutant *xi-1 xi-2 xi-i xi-k* displays impaired trafficking pathway responsible for the accumulation of PEN1 at the cell periphery. Strikingly, this mutant shows not only increased penetration rate but also enhanced overall disease susceptibility to both adapted and nonadapted fungal pathogens. Our findings establish myosins XI as key regulators of plant antifungal immunity.

actin cytoskeleton | plant immunity | endocytosis | vesicle | endocytic trafficking

In nature, plants are constantly exposed to a large number of pathogens including fungi, bacteria, and viruses. In response, plants have evolved multiple layers of defense mechanisms to resist the pathogen attack (1). The first line of plant defense against fungi is penetration resistance that is achieved by localized cell wall appositions (CWAs), also called papillae, on an inner surface of cell walls at the site of fungal penetration (2). CWAs consist primarily of callose (β-1,3-glucan), lignin, cell wall proteins, and reactive oxygen species (2–4). The focal deposition of these elements in papillae appears to be an early and essential factor in plant penetration resistance (5).

Studies on the genetic basis of penetration resistance have revealed that entry control of *A. thaliana* against nonadapted powdery mildews largely depends on several *PENETRATION* (*PEN*) genes (*PEN1*, *PEN2*, and *PEN3*). All three PEN proteins are also recruited to attempted fungal penetration sites (6–11). Intriguing findings show that the focal accumulation of PEN1 and PEN3 occurs outside the plasma membrane and within papillae or haustorial encasements (3, 11, 12). Disruption of actin cytoskeleton by pharmacological inhibitors blocks PEN3–GFP accumulation at most penetration sites, but has a lesser effect on the recruitment of GFP–PEN1 to these sites (11), suggesting that transport pathways mediating PEN1 and PEN3 recruitment and export to the apoplastic papillae are distinct.

Accumulation of dynamically moving cytoplasm near the pathogen penetration site is the most striking and microscopically visible early response in epidermal cells (2). The secretory vesicles and organelles, including peroxisomes, Golgi, mitochondria, and the nucleus, also move toward penetration sites (7, 13). In addition to the deposition of cell wall reinforcements and focal accumulation of penetration-related proteins such as PEN3, the accretion of cytoplasm and organelles at sites of attempted fungal penetration involves reorganization of actin cytoskeleton, which forms a radial array focused on penetration site (10, 11, 14–18). Consistent with this finding, disruption of AFs hampers penetration resistance, leading to increased penetration frequency by various fungal and oomycete pathogens (15–17, 19). However, the mechanisms that drive AF dynamics and active transport of cellular components toward sites of attempted pathogen penetration remain elusive. Myosins are molecular motors responsible for AF-based motility (20). Recently, plant class XI myosins were implicated in the organization of actin cytoskeleton, organelle and vesicle transport, cell expansion, and plant growth (21–27). Although none of the individual myosin gene knockouts produces plant growth defects (22), progressive elimination of two to four highly expressed myosins results in concomitant reduction in cell and plant size (23, 24). However, relatively little is known about the functions of myosins in plant–pathogen interactions (28, 29).

Using pharmacological and genetic approaches to disrupt myosin function in *Arabidopsis*, we show that transient assembly and polarization of actin filament (AF) bundles toward the fungal penetration site are regulated by myosin motors. Furthermore, we demonstrate that plant myosins contribute to focal aggregation of a battery of cellular defense activities at the infection site and papillary deposition of cell wall appositions of lignin-like compounds, callose and PEN1, and are required for plant penetration resistance.

Significance

Remodeling of actin cytoskeleton is thought to contribute to the establishment of effective barriers at the periphery of plant cells against fungal ingress. However, there is little information on the molecular mechanisms that regulate actin remodeling during interactions with invading pathogens. Here we show that disruption of myosin motors in *Arabidopsis* prevents dynamic reorganizations of actin filaments, focal organelle accumulation, and delivery of cell wall defense compounds toward the pathogen penetration site. Furthermore, the quadruple knockout mutant of class XI myosins exhibits impaired penetration resistance at the cell wall and enhanced overall disease susceptibility to both adapted and nonadapted fungal pathogens. This study provides insights into how myosins regulate cellular responses that contribute to plant immunity.

Author contributions: L.Y. and Y.W. designed research; L.Y., L.Q., G.L., and Y.W. performed research; V.V.P. and V.V.D. contributed new reagents/analytic tools; L.Y. and L.Q. analyzed data; and L.Y. and Y.W. wrote the paper.

The authors declare no conflict of interest.

This article is a PNAS Direct Submission.

[1]To whom correspondence should be addressed. Email: yangdou.wei@usask.ca.

This article contains supporting information online at www.pnas.org/lookup/suppl/doi:10.1073/pnas.1405292111/-/DCSupplemental.

Results and Discussion

Dynamics and Polarity of AF Bundles at the Pathogen Penetration Site. To gain insight into the AF dynamics in host cells in response to pathogen attack, we used transgenic *Arabidopsis* plants expressing ABD2–GFP, which permits acquisition of highly resolved F-actin images (30). Upon inoculation with conidiospores of a nonadapted barley powdery mildew, *Blumeria graminis* f. sp. *hordei* (*Bgh*), confocal microscopy revealed no difference in global AF dynamics between the noninfected and *Bgh*-attacked leaf epidermal cells at the early stages of appressorium-mediated infection. Strikingly, at ~9 h postinoculation (hpi), whereas the first microscopically detectable host cell response associated with cytoplasmic accretion occurred in the epidermal cell contacting attacking appressorium, AF polarization appeared toward the appressorial penetration site. The actin polarity was always coupled with AF bundle formation, with the long bundles radiating across epidermal cells (Fig. 1 and Movie S1). At 13–14 hpi, polarity with AF bundles appeared at over 45% of *Bgh*-attempted penetration sites and about 8% of those showed massive AF bundles pointing toward the infection site (Fig. 1). The polarity at various infection sites lasted for a period varying from 30 min to 3 h, and then the bundles gradually disassembled and the polarity disappeared accordingly. Once past the transition of polarization, free AFs reappeared and formed a dense, irregular patch of AFs adjacent to the *Bgh* penetration site, indicating that this focal adhesion region serves as binding sites for the AFs (Fig. 1).

To confirm that the ABD2–GFP marker faithfully reflects AF dynamics, we analyzed six transgenic *Arabidopsis* lines expressing GFP-tagged LIM proteins (GFP–WLIM1, GFP–WLIM2a, GFP–WLIM2b, GFP–PLIM2a, GFP–PLIM2b, and GFP–PLIM2c). The LIMs represent a distinct protein family with actin-binding domain unrelated to ABD2 (31). Although LIMs exhibited relatively high levels of diffuse cytoplasmic fluorescence compared with that of ABD2–GFP, cells expressing these GFP–LIMs showed AF organization and dynamic patterns in response to *Bgh* penetration similar to those in ABD2–GFP-expressing cells (Fig. S1). Because two nonhomologous types of actin-binding proteins revealed similar reorganization of AFs upon *Bgh* inoculation, we concluded that this pattern represents a bona fide host response rather than an artifact associated with the use of GFP-tagged reporters.

Myosin Inhibitors Compromise Penetration Resistance, AF Dynamics, and Organelle Trafficking. Myosins are molecular motors that upon interaction with AFs convert energy from ATP hydrolysis to generate force and motion. Because the rapid dynamic rearrangements of AFs at the *Bgh* penetration sites suggest possible involvement of myosins, we analyzed effects of myosin inhibitors on plant penetration resistance. As expected for the mock-treated control, *Bgh* appressoria mostly failed to penetrate leaf epidermal cells (Fig. 2*A*, H_2O control). Strikingly, penetration rates of *Bgh* appressoria in leaves infiltrated with two distinct myosin inhibitors, 2,3-butanedione monoxime (BDM) and *N*-ethylmaleimide (NEM), were increased dramatically, up to 10-fold, compared with control leaves (Fig. 2*A*). Because the increase in penetration efficiency was dose dependent for two chemically distinct myosin inhibitors, it can be assumed that myosins play an important role in penetration resistance.

Imaging analysis of leaf epidermal cells treated with myosin inhibitors showed that AFs appeared to be intact, but their dynamic rearrangements were markedly reduced. As evident from Fig. 2*B*, the focal polarization of AFs toward the *Bgh* penetration site was reduced, and no AF bundle formation was observed, indicating that myosin inhibition affected AF bundling and dynamics in response to pathogen attack.

Previous studies described aggregation of organelles at the pathogen penetration site (7, 10). Because organelle trafficking in plant cells relies on actomyosin motility, we further investigated the effects of myosin inhibitors on dynamic organelle behavior in response to *Bgh* attack. We first examined mitochondrial dynamics in leaf epidermal cells of *Arabidopsis* expressing mitochondrion-GFP marker (32) at *Bgh* penetration sites during the infection time course. Time-lapse confocal imaging revealed that mitochondrial aggregation toward the penetration sites was first observed at 9–10 hpi. Large numbers of mitochondria moved in several linear tracks and aggregated near the *Bgh* penetration site (Fig. 2 *C* and *D*). At 13 hpi, rapid migration of mitochondria toward penetration sites became most conspicuous with over 45% of the *Bgh*-attacked epidermal cells displaying mitochondrial aggregation. Thereafter, some mitochondria that had accumulated at the infection sites remained localized, surrounding the infection site. Examining *Arabidopsis* lines expressing markers of Golgi and peroxisomes (32), we found that trafficking patterns of these organelles were similar to that of mitochondria (Fig. S2*A*). Likewise, continuous streaming of the marker-tagged endoplasmic reticulum (ER) network and tonoplast resulted in increased accumulation of the corresponding endomembranes in the area adjacent to penetration site (Fig. S2*A*). Upon treatment with NEM, the rapid, long-distance, directional transport of organelles toward the infection site was severely suppressed; instead, saltatory movements over short distances occurred, which led to random organelle distribution in NEM-treated cells and only marginal accumulation at *Bgh* penetration sites (Fig. 2*D*, Fig. S2*A*, and Movies S2–S11). These results indicate that organelle accretion near the pathogen penetration site depends on action of myosin motors.

Recent studies suggested involvement of vesicle trafficking in cell wall appositions at fungal attack sites, although the identity and the cargo of these carrier vesicles remain unknown (9, 10, 33). We further examined effects of NEM treatment on the vesicle trafficking pathways, including transports of ARA6–GFP-tagged vesicles to plasma membrane (34), GFP–ARA7-tagged vesicles to multivesicular body (35), VHA-a1–GFP-tagged vesicles to *trans*-Golgi network (36), and GFP–VAMP727-tagged vesicles to vacuole (37). Each of these four vesicle classes aggregated toward the fungal attack site, indicating that localized delivery of a broad range of membrane-bound cargoes is triggered by penetration attempts. Moreover, NEM treatment prevented rapid movement and accumulation of these vesicles in a vicinity of attack sites, suggesting that targeted vesicle transport requires myosin motors (Fig. S2*B* and Movies S12–S19).

Collectively, these results indicate that the actomyosin motility system provides both the main tracks and the molecular motors for bulk aggregation of organelles and endomembrane vesicles near the *Bgh* penetration sites.

Focal Accumulation and Papillary Deposition of Cell Wall Appositions Are Affected by Myosin Inhibitor. To address a mechanistic basis of the myosin contributions to penetration resistance, we investigated

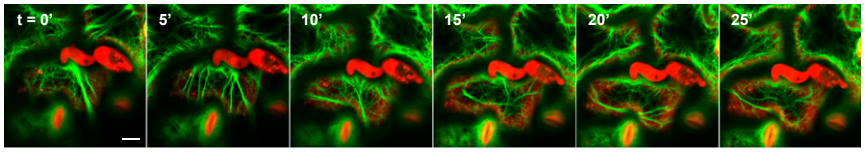

Fig. 1. Time-series image sequences showing polarization and bundle formation of actin filaments (AFs) toward the fungal penetration site. *Arabidopsis* leaves expressing 35S::GFP–ABD2–GFP were inoculated with *Bgh* conidiospores. Fungal conidium and appressorium were stained by propidium iodide (PI) (red). Confocal micrographs were taken from 0 to 25 min, beginning at 16 hpi. (Scale bar: 10 μm.)

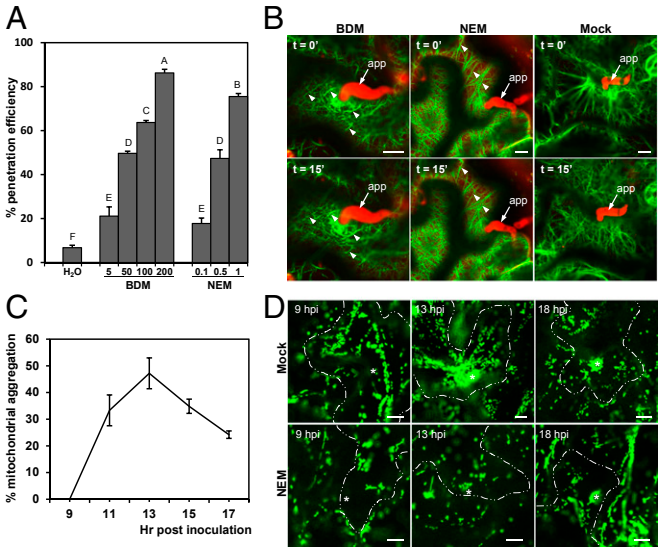

Fig. 2. Effects of myosin inhibitors on *Bgh* penetration, AF dynamics, and organelle movement. (*A*) Penetration efficiency of *Bgh*. Leaves of Col-0 were infiltrated with water, or myosin inhibitors, BDM (in millimoles) or NEM (in millimoles), and incubated for 1 h before inoculation with *Bgh* conidiospores. The frequency of fungal penetration was determined at 16 hpi by counting 150 interaction sites for each of a total of three leaves. Error bars represent SD ($n = 3$). (*B*) Dynamic rearrangement of AFs at the attempted penetration sites. Leaves expressing 35S::GFP–ABD2–GFP were infiltrated with water (mock), BDM (200 mM), or NEM (1 mM), and incubated for 1 h before inoculation with *Bgh*. At 16 hpi, leaf tissues were stained with PI (red) and examined under a confocal microscope. Arrowheads indicate the appearance of corresponding AFs between 15-min intervals. app, appressorium. (Scale bars: 10 μm.) (*C*) Time-course response of mitochondrial aggregation at the *Bgh* penetration sites. Data were collected by counting 150 *Bgh* attempted penetration sites for each of three independent experiment replicates at single time point. Means expressed as percentage of mitochondrial focal aggregation at various time points post *Bgh* inoculation. (*D*) Dynamic movements of mitochondria toward the *Bgh* penetration site. Leaves expressing mitochondrion-GFP were infiltrated with water or 1 mM NEM and subsequently inoculated with *Bgh*. At 9, 13, and 18 hpi, the infected epidermal cells indicated by dotted lines were examined by confocal microscopy. The stacked time-lapse images were captured with Z projections of five images. Asterisks indicate the *Bgh* penetration site in epidermal cells. (Scale bars: 10 μm.)

the effects of NEM treatment on integration of specific components of extracellular defense into the papillae and haustorial encasements (extracellular structures surrounding haustoria that are formed by papilla extension).

In particular, we monitored signals of the autofluorescent materials, indicative of accumulation of the phenolic, lignin-like compounds at fungal penetration sites of epidermal cells. At 36 hpi with *Bgh*, strong autofluorescence appeared in the papilla and surrounding halo area at an attempted penetration site, in the haustorial encasement, and in adjacent cell walls in mock-treated leaves (Fig. 3*A*). Upon NEM treatment, autofluorescence signal associated with these fungal attack sites was barely detectable. Thus, the increased *Bgh* penetration frequency in response to NEM treatment (Fig. 2*A*) was accompanied by dramatic reduction in the development of encasement surrounding the fungal haustorium (Fig. 3*A*). These results suggest that myosin inactivation prevents focal accumulation and deposition of autofluorescent materials into the papillary matrix.

We further investigated deposition of callose, an additional well-known constituent of the papillae and haustorial encasements (3, 9). At 16 hpi, epifluorescence imaging analysis revealed very bright and dense callose cores associated with the papilla matrix and haustorial encasement in mock-treated leaves (Fig. 3*B*). In leaves treated with NEM, only a relatively weak aniline blue fluorescence appeared in the peripheral zone surrounding the *Bgh* attempted penetration site and discrete callose dots aggregated toward the *Bgh* penetrated site (Fig. 3*B*). This experimental outcome suggested the involvement of myosin-dependent mechanism regulating callose depositions to the site of powdery mildew attack.

Next, we examined the PEN1 localization in transgenic *Arabidopsis* lines expressing GFP–PEN1 (38). Similar to lignin-like compounds and callose, intense GFP–PEN1 signals were detected within the interior of papillae and haustorial encasements in mock-treated epidermal cells, whereas the NEM-treatment rendered GFP–PEN1 signals into discrete dots around the *Bgh* penetration site, and blocked its accumulation in apoplastic papilla and around haustoria (Fig. 3*C* and Fig. S3 *A* and *B*).

Myosins XI Are Critical Components of Plant Antifungal Defense. The *Arabidopsis* genome encodes 4 myosins VIII and 13 myosins XI (39). To identify myosins responsible for penetration resistance in *Arabidopsis*, we first investigated the expression profiles of myosin genes in *Arabidopsis* leaves in response to the *Bgh* challenge (Fig. S4). The RT-PCR analyses revealed no significant induction for any of the 17 myosin genes in response to infection, suggesting that expression of myosin genes is constitutive (Fig. S4 and Table S1). Eight myosin genes are highly expressed in leaf tissue, including 5 myosin XI genes (*XI-1*, *XI-2*, *XI-H*, *XI-I*, and *XI-K*) and 3 myosin VIII genes (*VIII-1*, *VIII-2*, and *VIII-A*) (40). To determine specific contributions of the highly expressed myosins XI to penetration resistance, we screened a series of single

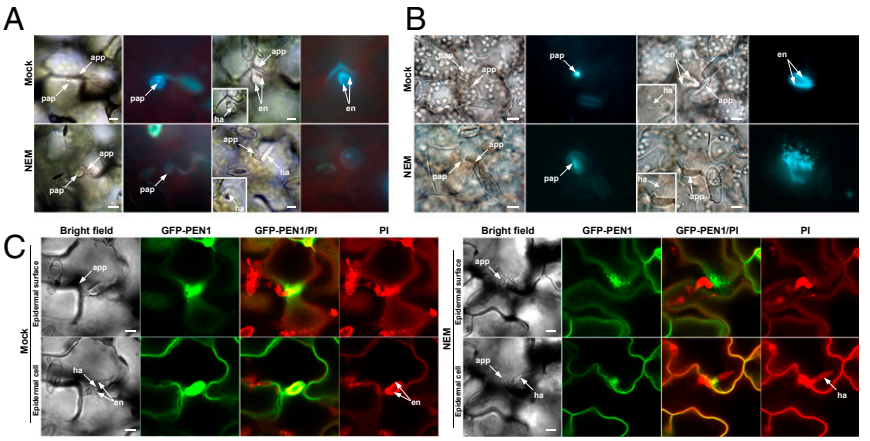

Fig. 3. Myosin inhibitor prevents focal accumulation and papillary deposition of cell wall materials. Leaves of Col-0 expressing PEN1::GFP–PEN1 infiltrated with water (mock) or 1 mM NEM were inoculated with *Bgh* conidiospores. (*A*) Accumulation and deposition of lignin-like compounds. The autofluorescence in both nonpenetrated (papillae) and penetrated (haustorial encasement) sites of fresh Col-0 leaves at 36 hpi was directly viewed by fluorescence microscopy. *Insets* depict close views of haustorial structures under transmitted light. (*B*) Accumulation and deposition of callose. The callose fluorescence in both nonpenetrated and penetrated sites of fixed and aniline blue-stained Col-0 leaves at 16 hpi was viewed by fluorescence microscopy. (*C*) Accumulation and deposition of GFP–PEN1. At 16 hpi, leaves of GFP–PEN1 plants were examined under a confocal microscope. Fungal conidia and appressoria were staining with PI (red). The same inoculation sites were viewed on the peripheral surface or into cells of the leaf epidermis. app, appressorium; en, haustorial encasement; ha, haustorium; pap, papilla. (Scale bars: 10 μm.)

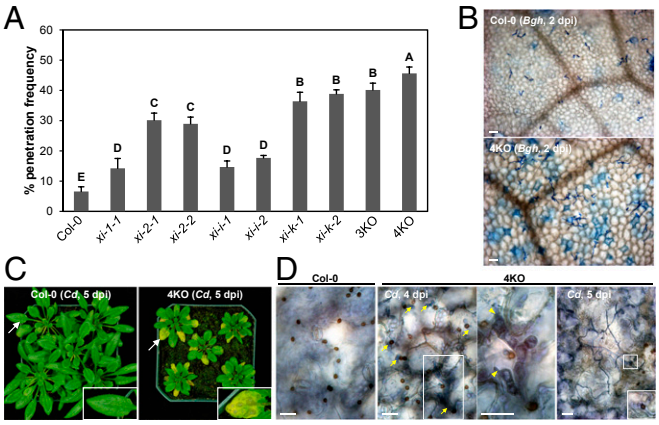

Fig. 4. Compromised penetration resistance of *Arabidopsis* myosin mutants against nonadapted fungal pathogens. (*A*) Quantitative analysis of penetration rates of nonadapted *Bgh* at 16 hpi on leaves of Col-0 and myosin single, triple, and quadruple mutants. At least 300 attempted penetration sites were scored for each genotype. (*B*) *Bgh* development on Col-0 and 4KO leaves. Inoculated leaves at 2 dpi were stained with aniline blue and examined. (Scale bars: 50 μm.) (*C*) Symptom development at 5 dpi after nonadapted *C. destructivum* (*Cd*) attack. *Insets* show symptom development on single leaves (indicated by arrows). (*D*) Microscopic symptom development after *Cd* attack. Leaves of Col-0 and 4KO were stained with Trypan blue after 4 or 5 dpi with *Cd*. Enlarged view shows the transition (arrowheads) from the biotrophic hyphae to the necrotrophic hyphae. *Inset* depicts surface view of the infection site. Arrows indicate primary hyphae. (Scale bars: 20 μm.)

and multiple gene knockout mutants for potential penetration alterations upon *Bgh* attack, including seven single mutants *xi-1-1*, *xi-2-1*, *xi-2-2*, *xi-i-1*, *xi-i-2*, *xi-k-1*, and *xi-k-2*, one triple mutant (3KO, *xi-1-1 xi-2-1 xi-k-2*), and one quadruple mutant (4KO, *xi-1-1 xi-2-1 xi-i-1 xi-k-2*) (Fig. S5 *A* and *B*). In each of the *xi-1*, *xi-2*, *xi-i*, and *xi-k* single knockout mutants, penetration rates at 2 dpi were from 2.2- to 5.9-fold higher than that in the Col-0 (Fig. 4*A*). The penetration rates for 3KO and 4KO were 40% and 46%, respectively, that is ∼6 to sevenfold increase relative to 6.5% penetration rate for Col-0 (Fig. 4*A*). These results indicated that each of the four tested myosin genes provides functionally redundant contributions to penetration resistance with myosin XI-K playing a predominant role. Interestingly, myosin XI-K also plays leading roles in transport of various organelles and in cell growth, whereas other highly expressed myosins XI provide redundant contributions to these processes (24, 25).

The low penetration rates of the nonadapted *Bgh* in Col-0 were accompanied by abortive infection with development of unilateral haustoria that were completely encased by extended papilla. The epiphytic elongation hyphae on the leaf surface were barely detectable (Fig. 4*B*), and *Bgh* infection did not progress beyond this stage. However, in the myosin 4KO mutant, *Bgh* infection resulted in the formation of a typical bilateral haustorium possessing numerous projections in penetrated epidermal cells, and the infected sites permitted sustained epiphytic hypha growth with the formation of microcolony of two to three elongating hyphae (Fig. 4*B* and Fig. S6). The progress of colonization usually ceased at this stage, indicating that impairment of the postinvasion resistance in myosin 4KO mutant was partial rather than complete.

We used another nonadapted fungal pathogen *Colletotrichum destructivum* (*Cd*) to further evaluate disease resistance of the myosin 4KO mutant. For this fungus, abundant conidial germination and appressorial formation were observed on leaf surface, but no visible symptom development and no invasive hyphae were detected in leaf epidermal cells of Col-0 plants (Fig. 4*C*), consistent with a previous report (41). In contrast, the 4KO mutant was fully susceptible to the *Cd* infection and displayed necrotic water soaking lesions on inoculated leaves at 5 dpi (Fig. 4*C*). Microscopic analysis revealed that abundant invasive primary hyphae appeared underneath the appressoria-mediated penetration sites, and switching of larger primary hyphae to thin necrotrophic secondary hyphae was associated with necrotic lesion development at 5 dpi (Fig. 4*D*). Taken together, the data on *Bgh* and *Cd* demonstrated that the highly expressed myosins XI function in both preinvasion and postinvasion resistance to two distinct nonadapted pathogenic fungi.

To determine the roles of myosins in the infection by *Arabidopsis*-adapted pathogenic fungi, we used *Erysiphe cichoracearum* (*Ec*) and *Colletotrichum higginsianum* (*Ch*). Compared with Col-0 plants, the myosin 4KO mutant inoculated with *Ec* displayed more fungal growth and hyphal branches at 2 dpi and more conidiophores at 7 dpi (Fig. S7 *A*–*C*). Likewise, inoculation with the hemibiotrophic *Ch* resulted in enhanced disease susceptibility in 3KO and 4KO mutants during the entire course of infection (Fig. S7*D*). Thus, myosins XI are critical components of plant defense against a wide spectrum of fungal pathogens.

Myosins XI Modulate Pathogen-Triggered Cell Wall Depositions. Because the myosin inhibitor treatments significantly impaired focal accumulation and deposition of callose and autofluorescent material at *Bgh* penetration sites, we sought to determine if the resistance-compromised myosin 4KO mutant also showed altered depositions of callose and autofluorescent material. A time-course study revealed that this mutant had a ∼1-h delay in the appearance of callose at the attempted *Bgh* penetration sites (Fig. 5 *A* and *B*). Similar delays in callose deposition were described for *pen1-1* and *gnom*$^{B/E}$ mutants (9, 12). In the penetrated epidermal cells of 4KO mutant at 48 hpi, callose depositions surrounded the collar regions of bilateral haustoria, whereas unilateral haustoria in penetrated epidermal cells of Col-0 were always trapped in callose encasements (Fig. S6). Furthermore, 4KO mutant showed significant reduction in recruitment of autofluorescent material to *Bgh* penetration sites relative to Col-0 (Fig. 5*C*). In the penetrated cells of Col-0, strong autofluorescent material depositions were detected in haustorial encasements, surrounding halo and adjacent cell walls. However, residual autofluorescent material depositions appeared only at the adjacent cell walls and collar regions of the multiprojected haustoria in absence of haustorial encasements. Thus, phenotypic analysis of the 4KO myosin mutant validated the data obtained using chemical inhibitors and established a role of specific myosins XI in pathogen-induced depositions of cell wall components.

Myosins XI Are Required for Maintaining Steady-State Level of PEN1. To evaluate the effect of myosins XI on PEN1 dynamics, we generated a 4KO *Arabidopsis* line stably expressing GFP–PEN1 (38). Confocal imaging revealed that the GFP–PEN1 signal intensity at cell periphery in this line was reduced to 19% of that in Col-0 (Fig. 6 *A* and *B*). After plasmolysis, the GFP–PEN1 fluorescence in Col-0 cells remained associated with the protoplast plasma membrane (PM) and was also visible in the PM extensions (Hechtian strands) connecting PM to the cell wall of plasmolyzed cells as reported previously (38). In contrast, only weak fluorescence appeared in the protoplasm, and the PM extensions labeled by FM4-64 and GFP–PEN1 were largely diminished in myosin 4KO (Fig. S8), suggesting that disruption of the PM-cell wall adhesion occurred in myosin 4KO.

We further examined the levels of transcript and protein accumulation in the leaves of Col-0 and 4KO lines expressing GFP–PEN1. It was found that the *GFP–PEN1* transcript levels were similar for the Col-0 and 4KO lines (Fig. 6*C*). However, significant reduction of the GFP–PEN1 protein accumulation was observed in 4KO mutant compared with Col-0 (Fig. 6*D*), suggesting that myosins XI are required to maintain normal level of PEN1 proteins in *Arabidopsis*.

In general, the steady-state levels of PM-resident proteins are regulated through the biosynthetic secretory and endocytic pathways (42) either of which could be affected in the 4KO mutant resulting in a substantial reduction of the steady-state

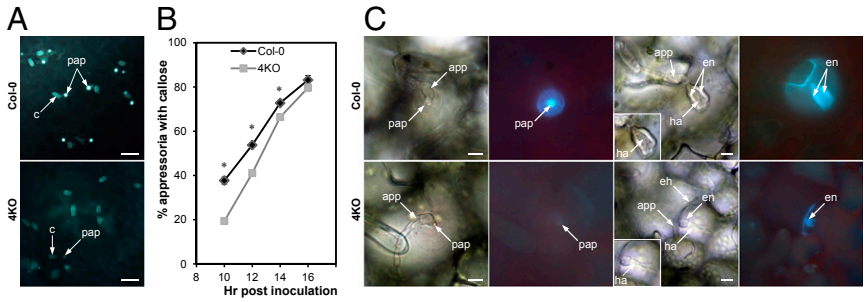

Fig. 5. Compromised deposition of callose and lignin-like compounds in myosin 4KO mutant in response to nonadapted *Bgh* attack. (*A*) Callose deposition at the *Bgh*-attempted penetration site of Col-0 and 4KO at 12 hpi. Leaves were stained with aniline blue and visualized by fluorescence microscopy. (Scale bars: 50 μm.) (*B*) Frequency of callose deposition at *Bgh* attack sites in a time course of 10–16 hpi. At least 150 germinated spores were scored for each sample. Error bars represent SD ($n = 3$). *$P < 0.01$. (*C*) Deposition of autofluorescent material at 36 hpi. The autofluorescence in both nonpenetrated (papilla, *Left* two panels) and penetrated (haustorial encasement, *Right* two panels) sites of Col-0 and 4KO was viewed by fluorescence microscopy. *Insets* depict close views of haustorial structures. app, appressorium; c, conidium; ha, haustorium; eh, elongation hypha; en, haustorial encasement; pap, papilla. (Scale bars: 10 μm.)

level of this protein. However, it is important to note that *Arabidopsis* PEN1 is associated with the pathogen-induced PM microdomains and exhibits constitutive cycling between the PM and endosomes (6, 9, 43). This striking dynamic behavior may facilitate rapid retargeting of PEN1 to the pathogen infection site. To investigate possible involvement of endocytic pathway in regulation of the GFP–PEN1 levels, we used the endocytic tracer FM4-64. Imaging analysis revealed extensive overlapping pattern for the FM4-64–labeled internalized membranes (endosome-like intermediate compartment) and the strong GFP–PEN1 signal at the periphery of Col-0 leaf epidermal cells (Fig. 6*E*). In contrast, only a small fraction of the FM4-64 signal overlapping with reduced GFP–PEN1 signal occurred in 4KO cells, suggesting that the endocytic transport of PEN1 was largely compromised in this myosin mutant (Fig. 6*E*).

To determine if the endocytic pathway for GFP–PEN1 recycling to the PM is indeed affected in myosin 4KO cells, brefeldin A (BFA) was used to disrupt the ARF–GEF GNOM activity and to retarget the endocytosed GFP–PEN1 to a BFA-induced compartment (BFA bodies) (9). Within 2 h upon BFA treatment, a substantial fraction of the GFP–PEN1 fluorescence colocalizing with FM4-64 signals appeared in large motile BFA bodies in almost Col-0 epidermal cells (Fig. 6*F*, arrowheads, *Upper Right*). In contrast, BFA-treated myosin 4KO epidermal cells retained most of GFP–PEN1 at the PM with the small, BFA-induced GFP–PEN1 aggregates firmly attached to PM (Fig. 6*F* and Movies S20 and S21). Upon simultaneous treatment of Col-0 leaves with BFA and protein synthesis inhibitor cycloheximide (Fig. S9), GFP–PEN1 colocalized with FM4-64 in BFA bodies similar to those shown in Fig. 6*F*. This result suggests that the GFP–PEN1 accumulating in these BFA bodies is not de novo synthesized, but rather derived from continuous recycling from the PM.

The defective GFP–PEN1 endocytic recycling in 4KO mutant could be due to impairment of either a general endocytosis or a specific GFP–PEN1 endocytic pathway. To distinguish between these possibilities, we quantified the FM4-64 internalized compartments in Col-0 and 4KO mutant with or without BFA treatment. Large numbers of endosome-like compartments (over 70 per cell) were observed in the leaf epidermal cells of Col-0, whereas only a few appeared in 4KO cells (Fig. S10 *A* and *B*). Consistent with a reduced general endocytosis rate, 4KO mutant also exhibited a dramatic reduction in the number and size of BFA bodies in leaf epidermal and root cells (Fig. S10 *C–E*). Collectively, these findings suggest that myosins XI are involved in a general endocytic pathway that modulates PEN1 levels at the PM. Potential role of myosins XI in the biosynthetic secretory pathway that might also contribute to the observed defects in GFP–PEN1 accumulation and distribution in 4KO mutant is a matter of future investigation.

It was also found that, upon inoculation with *Bgh*, inactivation of four myosins XI in 4KO mutant resulted in severe attenuation of GFP–PEN1 localization to the attempted penetration sites compared with that in Col-0 (Fig. S11 *A–C*). A similar effect of myosin inactivation was observed on the cell surface adjacent to the penetrated site where almost no signal was detected surrounding the haustorium in the absence of haustorial encasement in 4KO mutant (Fig. S11*D*). Taken together, these data indicate that the recruitment of PEN1 to the pathogen infection site and its steady-state level at the cell periphery are both controlled by activity of myosins XI.

Conclusions

In this report, we show that polarization of AF bundles toward the fungal penetration site in leaf epidermal cells involves precise

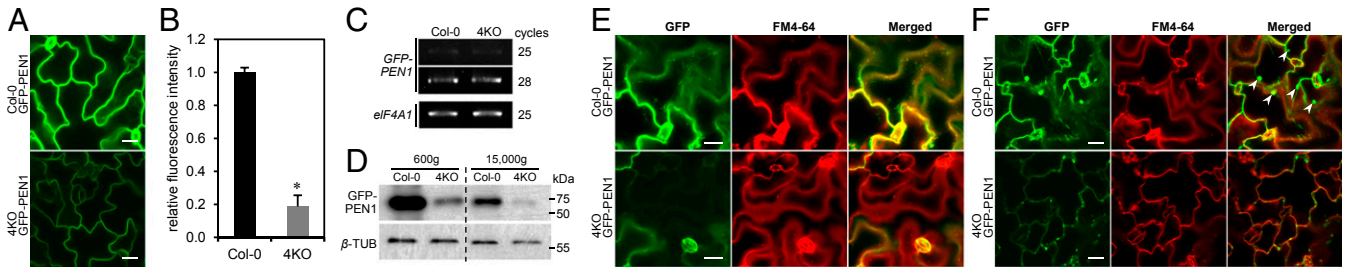

Fig. 6. Myosins XI regulate steady levels of PEN1. Four-week-old leaves of Col-0 and 4KO plants expressing PEN1::GFP–PEN1 were subjected to all analyses. (*A*) GFP–PEN1 signals captured with the same acquisition settings by focusing at anticlinal cell walls of leaf epidermal cells. (Scale bars: 50 μm.) (*B*) GFP–PEN1 fluorescence quantification at the cell periphery. Quantification was performed over three plants per each genotype. Error bars represent SD ($n = 45$). *$P <$ 0.01. (*C*) Semiquantitative RT-PCR of GFP–PEN1 construct. PCR products from two different cycles are shown for the GFP–PEN1 construct. The level of *eIF4A1* was used as an internal control to normalize amount of cDNA template. (*D*) Western blots of GFP–PEN1 proteins. Protein extracts fractioned by differential centrifugation to enrich for membrane (600 × *g*) and soluble (15,000 × *g*) proteins were probed with anti-GFP. β-Tubulin (β-TUB) was used for normalization. (*E*) GFP–PEN1 fluorescence and FM4-64 staining (red) signals on the periphery surface of leaf epidermal cells 1 h after loading FM4-64. (Scale bars: 20 μm.) (*F*) GFP–PEN1 signals in epidermal cells of leaf segments 2 h after 50 μM BFA treatment and FM4-64 staining. Arrowheads mark the BFA bodies with GFP–PEN1 and FM4-64 colocalizations. (Scale bars: 20 μm.)

spatiotemporal regulation. The resulting polarized AF arrays further mediate trafficking of organelles and carrier vesicles to the penetration site. Disruption of myosin activity by pharmaceutical inhibitors prevents pathogen-triggered AF reorganization and organelle movement leading to impaired papillary accumulation of cell wall components (callose, lignin-like compounds, and PEN1) and reduced penetration resistance. We also provide genetic evidence that the class XI myosins specifically contribute to cell wall-mediated penetration resistance presumably by driving the transport along the endocytic pathway.

Materials and Methods

A. thaliana plants of Col-0 ecotype and transgenic lines were grown in short day conditions. All T-DNA insertion lines were confirmed by PCR or sequencing analysis. Previously described adapted and nonadapted fungal pathogens on *Arabidopsis* were used in pathogenicity studies (41, 44). Chemical treatments included myosin inhibitors and inhibitors involved in endocytosis and protein synthesis. Plant and fungal tissues were examined by light, epifluorescence, or confocal microscopy. Additional details are included in *SI Materials and Methods*.

ACKNOWLEDGMENTS. We thank Paul Schulze-Lefert, Elison B. Blancaflor, Takashi Ueda, Clément Thomas, and Karin Schumacher for sharing materials that are important for this study; the *Arabidopsis* Biological Resource Center (Ohio State University) for providing seeds for *Arabidopsis* T-DNA insertion lines and transgenic marker lines; and Vipen Sawhney for critically reading the manuscript. This work was supported in part by grants from the Natural Sciences and Engineering Research Council of Canada (Discovery Grant), the Canadian Foundation for Innovation and Hubei Chutian Scholar Program (to Y.W.), and the Fundamental Research Funds for the Central Universities of China (Program 0900202175) (to L.Y.).

1. Thordal-Christensen H (2003) Fresh insights into processes of nonhost resistance. *Curr Opin Plant Biol* 6(4):351–357.
2. Aist JR (1976) Papillae and related wound plugs of plant cells. *Annu Rev Phytopathol* 14:145–163.
3. Meyer D, Pajonk S, Micali C, O'Connell R, Schulze-Lefert P (2009) Extracellular transport and integration of plant secretory proteins into pathogen-induced cell wall compartments. *Plant J* 57(6):986–999.
4. Thordal-Christensen H, Zhang ZG, Wei YD, Collinge DB (1997) Subcellular localization of H_2O_2 in plants. H_2O_2 accumulation in papillae and hypersensitive response during the barley-powdery mildew interaction. *Plant J* 11(6):1187–1194.
5. Hückelhoven R (2007) Cell wall-associated mechanisms of disease resistance and susceptibility. *Annu Rev Phytopathol* 45:101–127.
6. Bhat RA, Miklis M, Schmelzer E, Schulze-Lefert P, Panstruga R (2005) Recruitment and interaction dynamics of plant penetration resistance components in a plasma membrane microdomain. *Proc Natl Acad Sci USA* 102(8):3135–3140.
7. Koh S, André A, Edwards H, Ehrhardt D, Somerville S (2005) *Arabidopsis thaliana* subcellular responses to compatible *Erysiphe cichoracearum* infections. *Plant J* 44(3): 516–529.
8. Lipka V, et al. (2005) Pre- and postinvasion defenses both contribute to nonhost resistance in *Arabidopsis*. *Science* 310(5751):1180–1183.
9. Nielsen ME, Feechan A, Böhlenius H, Ueda T, Thordal-Christensen H (2012) *Arabidopsis* ARF-GTP exchange factor, GNOM, mediates transport required for innate immunity and focal accumulation of syntaxin PEN1. *Proc Natl Acad Sci USA* 109(28): 11443–11448.
10. Underwood W, Somerville SC (2008) Focal accumulation of defences at sites of fungal pathogen attack. *J Exp Bot* 59(13):3501–3508.
11. Underwood W, Somerville SC (2013) Perception of conserved pathogen elicitors at the plasma membrane leads to relocalization of the *Arabidopsis* PEN3 transporter. *Proc Natl Acad Sci USA* 110(30):12492–12497.
12. Assaad FF, et al. (2004) The PEN1 syntaxin defines a novel cellular compartment upon fungal attack and is required for the timely assembly of papillae. *Mol Biol Cell* 15(11): 5118–5129.
13. Böhlenius H, Mørch SM, Godfrey D, Nielsen ME, Thordal-Christensen H (2010) The multivesicular body-localized GTPase ARFA1b/1c is important for callose deposition and ROR2 syntaxin-dependent preinvasive basal defense in barley. *Plant Cell* 22(11):3831–3844.
14. Hardham AR, Jones DA, Takemoto D (2007) Cytoskeleton and cell wall function in penetration resistance. *Curr Opin Plant Biol* 10(4):342–348.
15. Kobayashi Y, et al. (1997) Dynamic reorganization of microfilaments and microtubules is necessary for the expression of non-host resistance in barley coleoptiles cells. *Plant J* 11(3):525–537.
16. Takemoto D, Jones DA, Hardham AR (2003) GFP-tagging of cell components reveals the dynamics of subcellular re-organization in response to infection of *Arabidopsis* by oomycete pathogens. *Plant J* 33(4):775–792.
17. Takemoto D, Jones DA, Hardham AR (2006) Re-organization of the cytoskeleton and endoplasmic reticulum in the *Arabidopsis pen1-1* mutant inoculated with the non-adapted powdery mildew pathogen, *Blumeria graminis* f. sp. *hordei*. *Mol Plant Pathol* 7(6):553–563.
18. Henty-Ridilla JL, Li J, Day B, Staiger CJ (2014) ACTIN DEPOLYMERIZING FACTOR4 regulates actin dynamics during innate immune signaling in *Arabidopsis*. *Plant Cell* 26(1):340–352.
19. Yun BW, et al. (2003) Loss of actin cytoskeletal function and EDS1 activity, in combination, severely compromises non-host resistance in *Arabidopsis* against wheat powdery mildew. *Plant J* 34(6):768–777.
20. Vale RD (2003) The molecular motor toolbox for intracellular transport. *Cell* 112(4):467–480.
21. Avisar D, Prokhnevsky AI, Makarova KS, Koonin EV, Dolja VV (2008) Myosin XI-K Is required for rapid trafficking of Golgi stacks, peroxisomes, and mitochondria in leaf cells of *Nicotiana benthamiana*. *Plant Physiol* 146(3):1098–1108.
22. Peremyslov VV, Prokhnevsky AI, Avisar D, Dolja VV (2008) Two class XI myosins function in organelle trafficking and root hair development in *Arabidopsis*. *Plant Physiol* 146(3):1109–1116.
23. Prokhnevsky AI, Peremyslov VV, Dolja VV (2008) Overlapping functions of the four class XI myosins in Arabidopsis growth, root hair elongation, and organelle motility. *Proc Natl Acad Sci USA* 105(50):19744–19749.
24. Peremyslov VV, Prokhnevsky AI, Dolja VV (2010) Class XI myosins are required for development, cell expansion, and F-Actin organization in *Arabidopsis*. *Plant Cell* 22(6):1883–1897.
25. Ueda H, et al. (2010) Myosin-dependent endoplasmic reticulum motility and F-actin organization in plant cells. *Proc Natl Acad Sci USA* 107(15):6894–6899.
26. Vidali L, et al. (2010) Myosin XI is essential for tip growth in *Physcomitrella patens*. *Plant Cell* 22(6):1868–1882.
27. Peremyslov VV, et al. (2013) Identification of myosin XI receptors in *Arabidopsis* defines a distinct class of transport vesicles. *Plant Cell* 25(8):3022–3038.
28. Harries PA, et al. (2009) Differing requirements for actin and myosin by plant viruses for sustained intercellular movement. *Proc Natl Acad Sci USA* 106(41):17594–17599.
29. Amari K, Lerich A, Schmitt-Keichinger C, Dolja VV, Ritzenthaler C (2011) Tubule-guided cell-to-cell movement of a plant virus requires class XI myosin motors. *PLoS Pathog* 7(10):e1002327.
30. Wang YS, Yoo CM, Blancaflor EB (2008) Improved imaging of actin filaments in transgenic *Arabidopsis* plants expressing a green fluorescent protein fusion to the C- and N-termini of the fimbrin actin-binding domain 2. *New Phytol* 177(2):525–536.
31. Papuga J, et al. (2010) *Arabidopsis* LIM proteins: A family of actin bundlers with distinct expression patterns and modes of regulation. *Plant Cell* 22(9):3034–3052.
32. Nelson BK, Cai X, Nebenführ A (2007) A multicolored set of *in vivo* organelle markers for co-localization studies in *Arabidopsis* and other plants. *Plant J* 51(6):1126–1136.
33. Feechan A, et al. (2013) Host cell entry of powdery mildew is correlated with endosomal transport of antagonistically acting VvPEN1 and VvMLO to the papilla. *Mol Plant Microbe Interact* 26(10):1138–1150.
34. Goh T, et al. (2007) VPS9a, the common activator for two distinct types of Rab5 GTPases, is essential for the development of *Arabidopsis thaliana*. *Plant Cell* 19(11): 3504–3515.
35. Jia T, et al. (2013) ARA7(Q69L) expression in transgenic *Arabidopsis* cells induces the formation of enlarged multivesicular bodies. *J Exp Bot* 64(10):2817–2829.
36. Dettmer J, Hong-Hermesdorf A, Stierhof YD, Schumacher K (2006) Vacuolar H^+-ATPase activity is required for endocytic and secretory trafficking in *Arabidopsis*. *Plant Cell* 18(3):715–730.
37. Ebine K, et al. (2008) A SNARE complex unique to seed plants is required for protein storage vacuole biogenesis and seed development of *Arabidopsis thaliana*. *Plant Cell* 20(11):3006–3021.
38. Collins NC, et al. (2003) SNARE-protein-mediated disease resistance at the plant cell wall. *Nature* 425(6961):973–977.
39. Reddy ASN, Day IS (2001) Analysis of the myosins encoded in the recently completed Arabidopsis thaliana genome sequence. *Genome Biol* 2:RESEARCH0024.
40. Peremyslov VV, et al. (2011) Expression, splicing, and evolution of the myosin gene family in plants. *Plant Physiol* 155(3):1191–1204.
41. Liu G, et al. (2007) Detached and attached *Arabidopsis* leaf assays reveal distinctive defense responses against hemibiotrophic *Colletotrichum* spp. *Mol Plant Microbe Interact* 20(10):1308–1319.
42. Richter S, Voss U, Jürgens G (2009) Post-Golgi traffic in plants. *Traffic* 10(7):819–828.
43. Reichardt I, et al. (2011) Mechanisms of functional specificity among plasma-membrane syntaxins in *Arabidopsis*. *Traffic* 12(9):1269–1280.
44. Liu G, et al. (2010) Amino acid homeostasis modulates salicylic acid-associated redox status and defense responses in *Arabidopsis*. *Plant Cell* 22(11):3845–3863.